

Optimization of endcap trap for single-ion manipulation

Yuan Qian(钱源), Chang-Da-Ren Fang(方长达人), Yao Huang(黄垚), Hua Guan(管桦), Ke-Lin Gao(高克林)
Citation: Chin. Phys. B . 2018, 27(6): 063701. **doi:** 10.1088/1674-1056/27/6/063701

Journal homepage: http://cpb.iphy.ac.cn; http://iopscience.iop.org/cpb

What follows is a list of articles you may be interested in

Quantitative evaluation of space charge effects of laser-cooled three-dimensional ion system on a secular motion period scale

Li-Jun Du(杜丽军), Hong-Fang Song(宋红芳), Shao-Long Chen(陈邵龙), Yao Huang(黄垚), Xin Tong(童昕), Hua Guan(管桦), Ke-Lin Gao(高克林)
Chin. Phys. B . 2018, 27(4): 043701. **doi:** 10.1088/1674-1056/27/4/043701

An optimized ion trap geometry to measure quadrupole shifts of ^{171}Yb+ clocks

N Batra, B K Sahoo, S De
Chin. Phys. B . 2016, 25(11): 113703. **doi:** 10.1088/1674-1056/25/11/113703

Determination of ion quantity by using low-temperature ion density theory and molecular dynamics simulation

Du Li-Jun, Song Hong-Fang, Li Hai-Xia, Chen Shao-Long, Chen Ting, Sun Huan-Yao, Huang Yao, Tong Xin, Guan Hua, Gao Ke-Lin
Chin. Phys. B . 2015, 24(11): 113703. **doi:** 10.1088/1674-1056/24/11/113703

Compensating for excess micromotion of ion crystals

Du Li-Jun, Chen Ting, Song Hong-Fang, Chen Shao-Long, Li Hai-Xia, Huang Yao, Tong Xin, Guan Hua, Gao Ke-Lin
Chin. Phys. B . 2015, 24(8): 083702. **doi:** 10.1088/1674-1056/24/8/083702

Implementation of ternary Shor's algorithm based on vibrational states of an ion in anharmonic potential

Liu Wei, Chen Shu-Ming, Zhang Jian, Wu Chun-Wang, Wu Wei, Chen Ping-Xing
Chin. Phys. B . 2015, 24(3): 033701. **doi:** 10.1088/1674-1056/24/3/033701

Optimization of endcap trap for single-ion manipulation*

Yuan Qian(钱源)[1,2,3], Chang-Da-Ren Fang(方长达人)[1,2,3], Yao Huang(黄垚)[1,2], Hua Guan(管桦)[1,2], and Ke-Lin Gao(高克林)[1,2,†]

[1] State Key Laboratory of Magnetic Resonance and Atomic and Molecular Physics, Wuhan Institute of Physics and Mathematics, Chinese Academy of Sciences, Wuhan 430071, China

[2] Key Laboratory of Atomic Frequency Standards, Wuhan Institute of Physics and Mathematics, Chinese Academy of Sciences, Wuhan 430071, China

[3] School of Physical Sciences, University of Chinese Academy of Sciences, Beijing 100049, China

(Received 27 December 2017; revised manuscript received 28 March 2018; published online 10 May 2018)

Potential distribution is an important characteristic for evaluating the performance of an ion trap. Here, we analyze and optimize the potential distribution of an endcap ion trap for single-ion trapping.We obtain an optimal endcap radius of 225 μm–250 μm, endcap-shield gap of ∼ 250 μm, and inter-endcap distance of 540 μm–590 μm. The simulation method for analysis can also be applied to other ion traps, which is useful for improving the design and assembly of ion traps.

Keywords: endcap ion trap, potential analysis, parameter optimization

PACS: 37.10.Ty, 41.20.–q, 42.62.Fi **DOI:** 10.1088/1674-1056/27/6/063701

1. Introduction

Ions trapped and laser-cooled in the radio-frequency (RF) field have been widely used in some areas, such as optical frequency standards (OFSs),[1–7] quantum information processing,[8–13] and quantum simulations.[14–17] In these applications, the structure of the ion trap is an important determinant of the ion trapping performance. For OFS applications, micro-motion is one of the main sources of system shifts, and it mainly depends on the trap parameters and assembly. Thus, it is very important to choose a suitable trap structure and parameters.[18] The endcap Paul trap is very suitable for single-ion trapping, because it has an open structure that enables laser access, its microscopic geometric structure is quite elaborate, and the fabrication process is relatively simple.

In the present work, we choose the endcap trap that was first proposed by Schrama *et al.*[19] with different geometric variants of the conventional quadrupole potential. We build a model of the endcap trap by using the commercial software COMSOL Multiphysics, simulate the potential distribution by using the finite element method, and derive optimal parameters. The main parameters of the physical model are adjusted to achieve the optimal manipulation of single ions. The trajectory of Sr^+ ions is then simulated, from which the secular motion and micro-motion frequency are predicted. The simulated results are compared with the experimental results obtained at the National Physical Laboratory (NPL).[20] Finally, the motion of a single Ca^+ ion, trapped in our vacuum chamber at a pressure of $\sim 10^{-8}$ Pa, can be simulated using our endcap trap model. The simulation results are used as a reference to study a directly laser-cooled Al^+ optical clock, which we are planning to build in the very near future; the current endcap trap model is envisioned to be a critical component of that future system.

2. Working principle and parameter optimization of the proposed ion trap

2.1. Working principle of the proposed ion trap

In an ion trap, the motion of a charged particle is limited by electric and magnetic fields. Ion traps can be divided into two main types, depending on the nature of the trapping field. One type is the Penning trap, which traps ions by using static electric and magnetic fields.[21] The other is the Paul trap, which traps ions by using RF alternating current (AC) electric potential fields at a level of a few megahertz.[22] The function of the Paul trap is determined by its structure. In this work, we focus on the endcap trap that is used primarily for trapping single ions, which is suitable for our experiments on the direct cooling of aluminum ions. As shown in Fig. 1, the tiny formation near the central area is an endcap made of molybdenum wires under an applied RF potential, and the shield electrode located over the endcap wires is made of tantalum tubes. Alumina tubes were inserted between the shield and endcap electrodes to provide electrical insulation and mechanical centering. To reduce the interaction between ions and background gases, the trap must operate in an ultra-high vacuum (UHV).

*Project supported by the National Key Research and Development Program of China (Grant No. 2017YFA0304401), the National Development Project for Major Scientific Research Facility, China (Grant No. ZDYZ2012-2), the National Natural Science Foundation of China (Grant Nos. 91336211 11634013, 11474318, and 11622434), the Strategic Priority Research Program of the Chinese Academy of Sciences (Grant No. XDB21030100), the Hubei Provincial Science Fund for Distinguished Young Scholars, China (Grant No. 2017CFA040), and the Youth Innovation Promotion Association, Chinese Academy of Sciences (Grant No. 2015274).

†Corresponding author. E-mail: klgao@wipm.ac.cn

© 2018 Chinese Physical Society and IOP Publishing Ltd

Earnshaw's theorem states that a collection of point charges cannot be maintained in a stable stationary equilibrium configuration solely by electrostatic interactions between the charges.[23] Thus, it is necessary to add an AC electric field on the electrodes:

$$\phi_0 = U + V\cos\Omega t, \tag{1}$$

where ϕ_0 is the excitation voltage on trap electrodes, U is the direct current (DC) voltage applied to the trap, and V is the zero-to-peak amplitude of the RF potential with an angular frequency of $\Omega = 2\pi f$, where f is the drive frequency of the signal generator. Ideally, the potential distribution in Fig. 1(b) can be achieved when U is set to be zero.

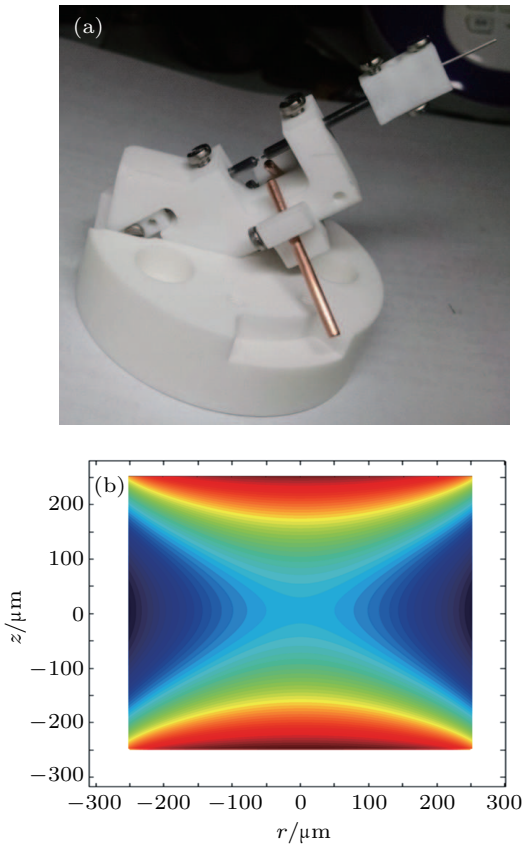


Fig. 1. (color online) (a) Photograph of the endcap used in our laboratory, and (b) potential distribution around the center of endcap.

The trap has rotational symmetry about the z axis, thus, the potential does not rely on angle φ.

When expressed in polar coordinates, the potential at the point (r,z) is given by[14]

$$\phi(\rho,\theta,\varphi) = \phi_0 \sum_{n=0}^{\infty} A_n \frac{\rho^n}{r_0^n} \mathrm{P}_n(\cos\theta). \tag{2}$$

where r_0 is a scaling factor, the values of A_n are weighting factors, and the expressions P_n are Legendre polynomials of order n.

Taking n values of 2 to 6, we obtain

$$\begin{aligned}\phi_{r,z} = \phi_0\Bigg(&A_2\frac{r^2-2z^2}{2r_0^2} + A_3\frac{3r^2z-2z^3}{2r_0^3} \\ &+A_4\frac{3r^4-24r^2z^2+8z^4}{8r_0^2} \\ &+A_5\frac{15r^4z-40r^2z^3+8z^5}{8r_0^5} \\ &+A_6\frac{5r^6-90r^4z^2+120r^2z^4-16z^6}{16r_0^6}\Bigg).\end{aligned} \tag{3}$$

For the r direction, when $z = 0$, the potential is

$$\phi_r = C_{0r} + C_{2r}r^2 + C_{4r}r^4 + C_{6r}r^6 + \cdots \tag{4}$$

Otherwise, along the z axis, the potential is given by

$$\begin{aligned}\phi_z = &C_{0z} + C_{1z}z^1 + C_{2z}z^2 + C_{3z}z^3 \\ &+C_{4z}z^4 + C_{5z}z^5 + C_{6z}z^6 + \cdots\end{aligned} \tag{5}$$

Taking symmetry into consideration, the potential along the z axis can be written as

$$\phi_z = C_{0z} + C_{2z}z^2 + C_{4z}z^4 + C_{6z}z^6 + \cdots. \tag{6}$$

For simplicity, we denote the second term of the potential by b while its third term is represented by c. For example, b_r represents C_{2r} in Eq. (4), and c_z represents C_{4z} in Eq. (5). We use here the same method as the one used by Cao *et al.*[24] to determine the trap quality; the parameter b is used to evaluate the depth of the pseudopotential, and the ratio c/b is used to estimate the trap anharmonic potential. The potential distribution is calculated to obtain a set of data. Then, equations (4) and (6) are fitted by using the data to derive the corresponding coefficients for determining the trap quality.

As we mentioned above, the endcap trap possesses rotational symmetry about the z axis. The ion has the same motion trajectory at any arbitrary plane along the z axis. The ion motion can be confined roughly in a two-dimensional (2D) plane. At this point, the simulation can be simplified without affecting the results. After building the geometric model, a corresponding voltage is applied to the resulting trap model.

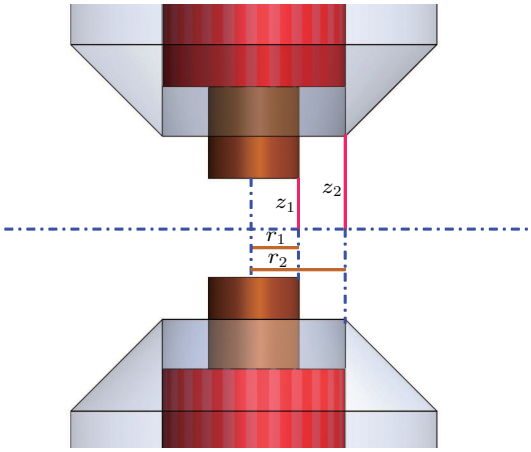


Fig. 2. (color online) Geometric structure of the endcap trap. r_1: endcap radius; r_2: shield radius; z_1: distance from the surface of the endcap to the geometric center; z_2: distance from the top to the center. r_1, r_2, z_1, and z_2 can be modified by the parameter sweep function in the COMSOL program.

The geometric structure of the endcap trap is shown in Fig. 2. We chose 25 μm as the sweeping step on the basis of the mesh. With respect to machining, 25 μm is a relatively small value in comparison with the trap's size, which is about 500 μm.

2.2. Parameter optimization of endcap ion trap

Before simulating the trap's potential, a test simulation was conducted to probe the performance of the software. A parallel capacitor was considered by using the software as shown in Fig. 3. The two electrodes were separated by 0.4 m in the parallel capacitor; the voltage on one of the electrodes was 50 V while the voltage on the other one was 0 V. A positive ion with the elementary charge and mass of 40 atomic mass units (Ca^+) was positioned at the center of the capacitor and was given an initial velocity of 10^4 m/s toward the 50 V electrode. We used the software to calculate the time from the moment of the ion release until the moment when its velocity reached 0 m/s. The calculated time is consistent with the theoretical value, up to a nanosecond. This model is simple but necessary. It is useful for checking whether the AC model performs satisfactorily at a given mesh resolution. It also helps to prove that the particle trajectory model is coupled well with the AC model.

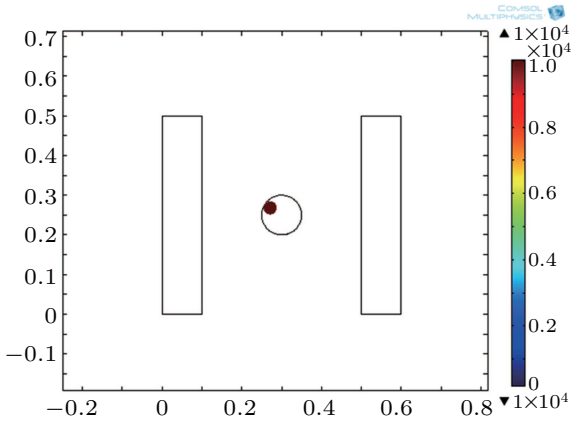


Fig. 3. (color online) Graphical presentation of the simulation of the Ca^+ ion's motion in planar plate capacitor.

The most important part of the simulation is mesh division, the quality of which is limited by our computing capability. Using COMSOL and MATLAB, we can also precisely control each mesh node and assess the details of the mesh quality distribution. The average statistical mesh quality was 0.97, initially at 0.85. We also built some mesh-controlled virtual geometry near the saddle point, where ions generally remained, to increase the resolution of the mesh. This procedure is advantageous for mesh division and does not affect the results of simulation.

Next, the parameters were optimized.

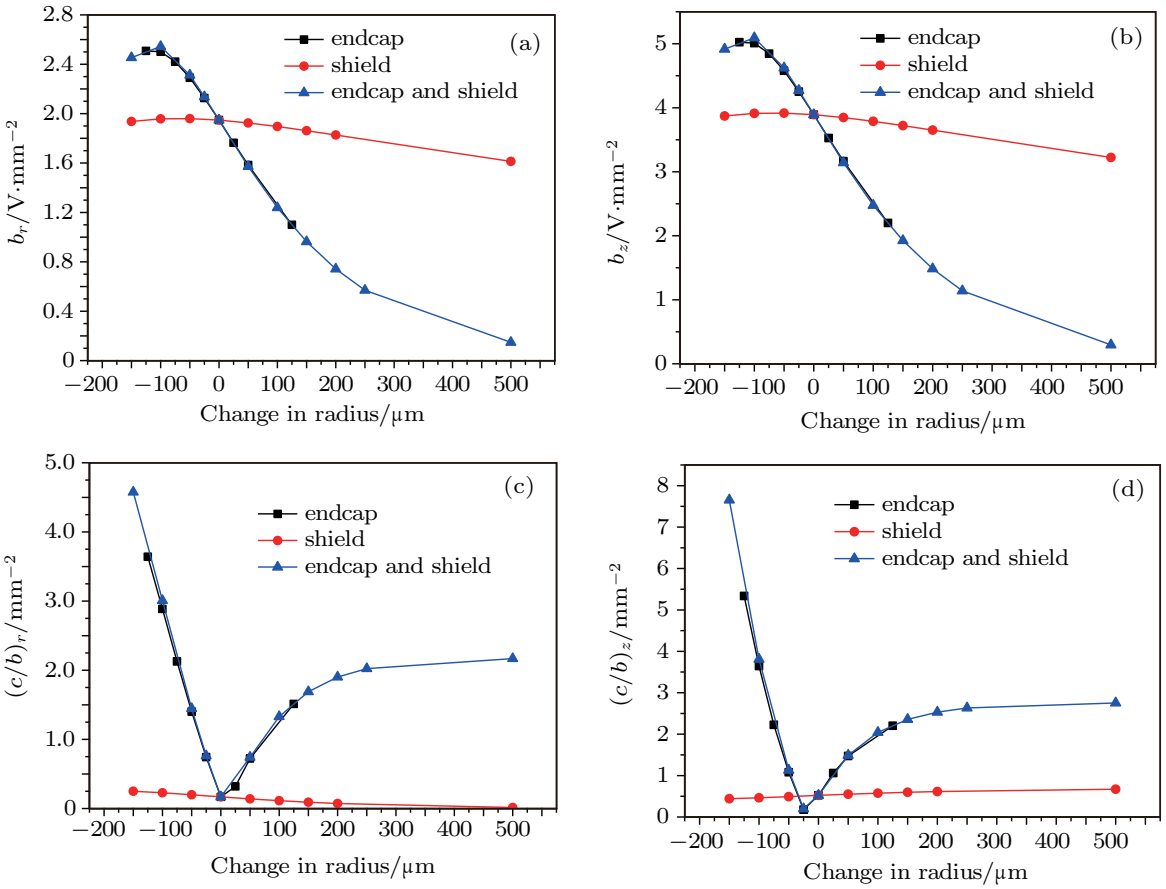


Fig. 4. (color online) Plots of ((a) and (b)) trap depth versus radius and ((c) and (d)) anharmonic coefficient versus radius. The black, red, and blue lines represent the endcap radius, shield radius, and both radii, respectively.

First, the radius of the device was varied. We changed r_1 alone, r_2 alone, and r_1 and r_2 simultaneously. The initial radius of the endcap, r_1, was set to be 250 μm, and the initial radius of the shield surrounding the endcap, r_2, was set to be 500 μm. We varied r_1 from 125 μm to 375 μm in steps of 25 μm, and we varied r_2 from 350 μm to 700 μm; further, 1000 μm was set as a far point, for examining a relatively extreme situation. In Fig. 4, the x axis represents a change in the radius, and the y axis represents b or c/b. Figure 4 reveals that only changing the shield radius has little effect on the trap potential depth or trap potential anharmonicity. On the other hand, the potential depth and potential anharmonicity fluctuate obviously when only r_1 changes. This may explain why the blue and black curves overlap. From these four plots, we concluded that the optimal endcap radius is in the range of 225 μm–250 μm. Further, the shield radius or the gap between the endcap and shield was found to have little effect on the potential distribution.

Second, the distances from the trap center to the endcap tip and from the trap center to the shield tip were varied. Three situations were considered: 1) moving only the endcap, 2) moving only the shield, and 3) moving the endcap and the shield simultaneously. By analyzing the results, the range of distances by which the two components of the trap should be separated was determined.

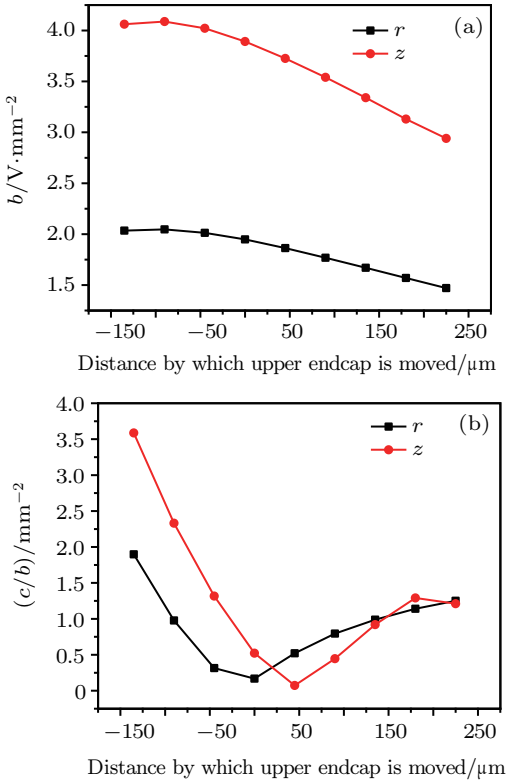


Fig. 5. (color online) Plots of (a) trap depth and (b) anharmonic coefficient versus distance upper endcap moves for various endcap locations.

Figure 5 shows the results for varying the upper endcap. In Fig. 5(a), the coefficient b increases as the upper endcap moves closer to the lower endcap. This phenomenon is easy to understand. The voltage on the endcap is fixed; when the endcaps approach to each other, the electric field increases, and so does the potential depth. There is an obvious relationship between r and z, which shows that the value of b in the r direction is about half the value in the z direction. In Fig. 5(b), the inflection points appear in both the r and z directions when the upper endcap moves upward. These points indicate the optimal position of the upper endcap and show that the upper endcap should be 0 μm–50 μm far from the lower endcap.

Figure 6 shows the results obtained when both endcaps moved simultaneously. The horizontal axis represents the distance the endcap moves; positive values indicate that the endcaps moves apart, and negative values refer to the endcaps moving in the opposite direction. Figure 6(a) shows that the potential depth does not increase indefinitely as the two endcaps approach to each other. In fact, the potential depth can be adjusted manually by changing the endcap voltage. Further, we prefer a longer distance between the two endcaps for easier access to the laser. Thus, the ratio c/b is of higher concern than b. Figure 6(b) shows that both endcaps should move 0 μm–25 μm apart from the center for optimal results. This result is in agreement with the result obtained by moving only one endcap, which shows that one of the endcaps should move 50 μm. The difference is caused by the loss of symmetry in the former case.

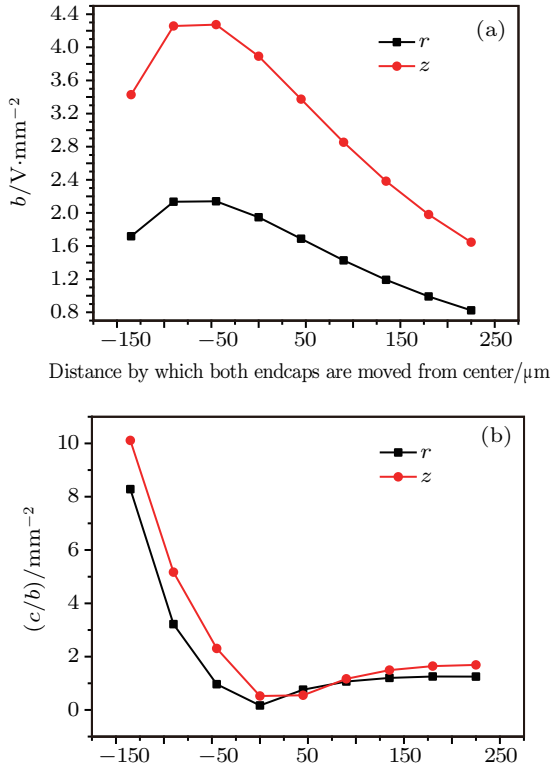


Fig. 6. (color online) Curves of (a) trap depth and (b) anharmonic coefficient versus distance endcap moves from center.

We obtained optimized trap parameters from the simulation. Based on the simulation, for optimal performance the ra-

dius of the endcap should be in the range of 225 μm–250 μm. Further, the gap between the endcap and the shield should be kept at ∼ 250 μm. In addition, the distance between the two endcaps should be in the range of 540 μm–590 μm.

Imperfections were also considered, such as the rotation of the endcaps at a specific angle with respect to the z direction, a shift of the endcap away from the trap axis, and the replacement of the mirror surface of the endcaps with a triangular wave, hollow semicircle, or nipple. The result for an imperfect endcap trap shows that the ratio c/b changes little compared with that for the flawless trap, but the effect is not negligible.

For comparison, experimental data from NPL were used in the ion trajectory simulation. The RF voltage was set to be 199 V (rms), and the frequency was set to be 15.955 MHz. The DC voltage applied to the shield was 2.12 V. The endcaps each with a radius of 250 μm were separated by 560 μm. The shields were separated by 1 mm and angled at 45° with respect to the trap axis. An $^{88}Sr^{+}$ ion was loaded with an initial kinetic energy of 0.05 eV from the center of the trap, with its velocity direction chosen randomly. The COMSOL has a particular particle trajectory node that is used to simulate the motion of charged particles in magnetic and electric fields. Another three-dimensional (3D) model was built in COMSOL by using the above parameters for a particle trajectory node. The motion data were exported and organized to calculate the secular frequencies. The secular frequencies were calculated to be 1.406 MHz in the r direction and 2.907 MHz in the z direction respectively, which were in good agreement with the NPL experimental results.[20]

3. Conclusion and perspective

In this work, an AC model has been used to simulate the endcap in the Paul trap, and the optimal trap parameters have been obtained. According to our results, the radius of the endcap should be in the range of 225 μm–250 μm, and the gap between the endcap and the shield should be ∼ 250 μm. Further, the distance between the two endcaps should be in the range of 540 μm–590 μm. These theoretical results can be used to guide experiments; for example, for designing the Ca^{+} ion optical clock that we are currently developing, and for designing a directly laser-cooled Al^{+} optical clock that we are to build in the near future. Further, the module can be used to determine the scale of the voltage applied to the compensation electrode to provide the ions with better trapping conditions. As COMSOL can also simulate the laser, it will be feasible in the next step to simulate the Doppler cooling of ions in the trap if we can build a two-level energy state model of the trapped ion. This function is not yet supported by the COMSOL module; however, we can formulate its associated partial differential equation by using COMSOL or MATLAB script. Furthermore, a heat module can be added to the model to obtain a more realistic situation. The heat module can be used to simulate the temperature of the trap and the surroundings to evaluate the blackbody radiation frequency shift in the OFS.

Acknowledgment

We thank Xin Tong and Jian Cao for their fruitful discussions, and Chengbin Li for helpful comments on the manuscript.

References

[1] Chou C W, Hume D B, Koelemeij J C J, Wineland D J and Rosenband T 2010 *Phys. Rev. Lett.* **104** 070802
[2] Dube P, Madej A A, Shiner A and Jian B 2015 *Phys. Rev. A* **92** 042119
[3] Godun R M, Nisbet-Jones P B, Jones R J M, King S A, Johnson L A M, Margolis H S, Szymaniec K, Lea S N, Bongs K and Gill P 2014 *Phys. Rev. Lett.* **113** 210801
[4] Huang Y, Cao J, Liu P, Liang K, Ou B, Guan H, Huang X, Li T and Gao K 2012 *Phys. Rev. A* **85** 030503
[5] Rosenband T, Hume D B, Schmidt P O, Chou C W, Brusch A, Lorini L, Oskay W H, Drullinger R E, Fortier T M, Stalnaker J E, Diddams S A, Swann W C, Newbury N R, Itano W M, Wineland D J and Bergquist J C 2008 *Science* **319** 1808
[6] Huntemann N, Sanner C, Lipphardt B, Tamm C and Peik E 2016 *Phys. Rev. Lett.* **116** 063001
[7] Margolis H S 2009 *Eur. Phys. J. Special Topics* **172** 97
[8] Michael Brownnutt 2007 "$^{88}Sr^{+}$ ion trapping techniques and technologies for quantum information processing", Ph. D dissertation (London: Imperial College London)
[9] Leibfried D, Knill E, Seidelin S, Britton J, Blakestad R B, Chiaverini J, Hume D B, Itano W M, Jost J D, Langer C, Ozeri R, Reichle R and Wineland D J 2005 *Nature* **438** 639
[10] Roos C, Zeiger T, Rohde H, Nägerl H C, Eschner J, Leibfried D, Schmidt-Kaler F and and Blatt R 1999 *Phys. Rev. Lett.* **83** 4713
[11] Blatt R and Wineland D 2008 *Nature* **453** 1008
[12] Monroe C and Lukin M 2008 *Phys. World* **21** 8
[13] Häffner H, Roos C F and Blatt R 2008 *Phys. Rep.* **469** 155
[14] March R E and Todd J F J 2005 *Quadrupole Ion Trap Spectrometry*, 2nd edn. (New Jersey: John Wiley & Sons, Inc.) pp. 93–94
[15] Chen T, Du L J, Song H F, Liu P L, Huang Y, Tong X, Guan H and Gao K L 2014 *Chin. Phys. B* **23** 123702
[16] Du L J, Chen T, Song H F, Chen S L, Li H X, Huang Y, Tong X, Guan H and Gao K L 2015 *Chin. Phys. B* **24** 083702
[17] Du L J, Song H F, Li H X, Chen S L, Chen T, Sun H Y, Huang Y, Tong X, Guan H and Gao K L 2015 *Chin. Phys. B* **24** 113703
[18] Huang Y, Guan H, Liu P, Bian W, Ma L, Liang K, Li T and Gao K 2016 *Phys. Rev. Lett.* **116** 013001
[19] Schrama C A, Peik E, Smith W W and Walther H 1993 *Opt. Commun.* **101** 32
[20] Brkic B, Taylor S, Ralph J F and France N 2006 *Phys. Rev. A* **73** 012326
[21] Brown L S and Gabrielse G 1986 *Rev. Mod. Phys.* **58** 233
[22] Wolfgang Paul 1990 *Rev. Mod. Phys.* **62** 531
[23] Earnshaw and Samuel 1842 *Trans. Camb. Phil. Soc.* **7** 97
[24] Cao J, Tong X, Cui K F, Shang J J, Shu H L and Huang X R 2014 *Chin. Phys. Lett.* **31** 043701